

doi: 10.12029/gc20200303

宋哲, 李厚民, 李立兴, 丁建华, 孟洁. 2020. 新疆东天山黑尖山铁矿床富铁团块中磁铁矿的成分特征及岩浆-热液演化过程[J]. 中国地质, 47(3): 590–606.

Song Zhe, Li Houmin, Li Lixing, Ding Jianhua, Meng Jie. 2020. Magnetite compositions of the iron-rich agglomerates of the Heijiashan iron deposit in Eastern Tianshan Mountains and magmatic-hydrothermal evolution processes[J]. Geology in China, 47(3): 590–606(in Chinese with English abstract).

新疆东天山黑尖山铁矿床富铁团块中磁铁矿的成分特征及岩浆-热液演化过程

宋哲^{1,2}, 李厚民¹, 李立兴¹, 丁建华¹, 孟洁³

(1. 自然资源部成矿作用与资源评价重点实验室/中国地质科学院矿产资源研究所, 北京 100037; 2. 地质过程与矿产资源国家重点实验室/中国地质大学(武汉), 湖北 武汉 430074; 3. 中国地质调查局发展研究中心, 北京 100037)

提要:黑尖山铁矿床是新疆东天山阿齐山—雅满苏成矿带中典型的海相火山岩型铁矿床。黑尖山矿床围岩安山质熔岩中发育大量不规则的富铁团块, 可分为钠长石磁铁矿型、钠长石钾长石磁铁矿型、钾长石磁铁矿型、绿帘石磁铁矿型和石英磁铁矿型5种类型, 可能代表了在岩浆-热液成矿过程中不同演化阶段的产物, 对黑尖山铁矿床成矿过程及形成环境有指示意义。本文对上述5类富铁团块中的磁铁矿进行了主量元素分析, 为了精确地测出磁铁矿中铁的总量, 采用差分法加入不确定的O含量, 并加以ZAF矩阵校正。对比5类富铁团块中磁铁矿Ti含量, 钠长石磁铁矿型最高, 钠长石钾长石磁铁矿型和钾长石磁铁矿型较高, 绿帘石磁铁矿型和石英磁铁矿型最低, 且Ti含量与Fe含量为正相关关系; 绿帘石磁铁矿型和石英磁铁矿型富铁团块Fe含量特征与矿石中磁铁矿Fe含量相近。上述特征表明钠长石磁铁矿类型是残余富铁熔体中最早的结晶产物, 钠长石钾长石磁铁矿和钾长石磁铁矿类型具有岩浆热液转变的特征, 而绿帘石磁铁矿和石英-磁铁矿类型则是受热液完全交代的产物, 说明矿床形成于岩浆-热液成矿作用。各类富铁团块内磁铁矿的Fe含量均大于相对应蚀变环边磁铁矿的Fe含量, 表明富铁岩浆结晶与热液活动分异同期发生。

关 键 词:海相火山岩型铁矿; 黑尖山; 富铁团块; 岩浆-热液; 矿产资源勘查工程; 东天山

中图分类号:P618.31 文献标志码:A 文章编号:1000-3657(2020)03-0590-17

Magnetite compositions of the iron-rich agglomerates of the Heijiashan iron deposit in Eastern Tianshan Mountains and magmatic-hydrothermal evolution processes

SONG Zhe^{1,2}, LI Houmin¹, LI Lixing¹, DING Jianhua¹, MENG Jie³

(1. MNR Key Laboratory of Metallogeny and Mineral Assessment, Institute of Mineral Resources, Chinese Academy of Geological Sciences, Beijing 100037, China; 2. Faculty of Earth Resources, China University of Geosciences, Wuhan 430074, Hubei, China;
3. Development and Research Center of China Geological Survey, Beijing 100037, China)

收稿日期:2019-09-27; 改回日期:2020-04-15

基金项目:中国地质调查局项目(DD20190606)和国家自然科学基金项目(41672078, 41272102)联合资助。

作者简介:宋哲,男,1990年生,博士生,从事金属矿床研究工作; E-mail:ddsz.2007@163.com。

Abstract: The Heijiashan iron deposit represents a typical submarine volcanic rock-hosted deposit of the Aqishan-Yamansu ore belt in Eastern Tianshan Mountains. Abundant irregular iron-rich agglomerates are developed in the brecciated andesite lava (wall rock), and they can be subdivided into five types, i.e., albite-magnetite type, albite-K-feldspar magnetite type, K-feldspar-magnetite type, epidote-magnetite type and quartz-magnetite type, likely representing evolving products of the magmatic-hydrothermal ore-forming process, which can constrain the ore-forming process and metallogenetic environment of the Heijiashan iron deposit. Magnetite compositions of the five types of agglomerates were analyzed using electron microprobe analysis. For the purpose of obtaining precise Fe content, the content of undetermined O was added by difference method and the ZAF matrix correction was conducted. The Ti values of the five types of agglomerates display a positive relationship with the Fe values. Magnetite of the albite-magnetite type has highest Ti content, the albite-K-feldspar magnetite and the K-feldspar-magnetite types show medium Ti content, whereas the epidote-magnetite and quartz-magnetite types are characterized by the lowest Ti content. Also, the Fe content of the epidote-magnetite and the quartz-magnetite types is similar to that of the ores. These features indicate that the albite-magnetite type seems to have been the earliest crystallization product from a residual iron-rich melt, the albite-K-feldspar-magnetite and K-feldspar-magnetite types display features of magmatic-hydrothermal transition, whereas the epidote-magnetite and quartz-magnetite types represent products of hydrothermal alteration. The Fe content of magnetite of each type of agglomerate is higher than its content of the corresponding alteration zone, suggesting a simultaneous relationship between the crystallization of iron-rich agglomerates and hydrothermal activities.

Keywords: submarine volcanic rock-hosted iron deposit; Heijiashan; iron-rich agglomerates; magmatic-hydrothermal; mineral resources exploration project; Eastern Tianshan Mountains

About the first author: SONG Zhe, male, born in 1990, doctor candidate, engages in the study of ore deposits; E-mail: ddsz.2007@163.com.

Fund support: Supported by China Geological Survey Program (No.DD20190606) and National Natural Science Foundation of China (No.41672078, No.41272102).

1 引言

与火山岩-次火山岩有关的火山岩型铁矿床赋存有巨量的铁矿石资源,并且常常形成富铁矿床,长期以来一直是研究热点(Porter, 2002; Williams et al., 2005)。火山岩型铁矿可进一步分为与陆相火山岩-次火山岩有关的含磷灰石铁氧化物矿床和产于海相火山-沉积岩系中的铁矿床两种亚类(李厚民等, 2012; Zhang et al., 2014; Li et al., 2015a; 张招崇等, 2016; 赵宏军等, 2018)。前者即著名的基鲁纳(Kiruna)型铁矿,在中国被称为玢岩型或陆相火山岩型铁矿,典型矿床有瑞典基鲁纳、智利拉科以及中国宁芜地区玢岩型铁矿(段超等, 2012; 王铁柱等, 2014);后者在中国新疆东、西天山广泛发育,典型矿床有智博、查岗诺尔和雅满苏铁矿等(曾红等, 2014; 王大川等, 2014; 陈杰等, 2014; 李潇林斌等, 2014; 段士刚等, 2014; 张振亮等, 2015)。铁的成矿与火山岩浆活动密切相关,又普遍受到热液交代蚀变的影响,因此矿床成因饱受争议,有矿浆成因(Park, 1961; Nyström et al., 1994; Naslund et al.,

2000; Naslund et al., 2002; Tornos et al., 2011; Tornos et al., 2016; Velasco et al., 2016),热液交代成因(Hildebrand, 1986; Rhodes et al., 1999; Gleason et al., 2000; Sillitoe et al., 2002; Barton, 2014)和岩浆-热液过渡成因(侯通等, 2010; Zhou et al., 2013; 李延河等, 2014; Knipping et al., 2015)观点。

近来笔者在东天山铁矿床研究工作中,在雅满苏、沙泉子、黑尖山等多个矿区均发现有富铁团块,这些团块分布在矿体围岩火山熔岩、火山碎屑岩中,形状不规则,内部具有明显的斑晶-基质结构、交织结构和气孔杏仁构造,显示典型的矿浆冷凝结晶成因的结构构造特点(Li et al., 2015, 2018)。富铁团块除可直接构成铁矿体外,也为后期热液改造富集形成富铁矿准备了物质基础。雅满苏铁矿中富铁团块可分为更长石磁铁矿型、更长石钠长石磁铁矿型、钠长石磁铁矿型、钠长石钾长石磁铁矿型和钾长石磁铁矿型,热液交代作用仅在富含钾长石的富铁团块中较发育(Li et al., 2015)。黑尖山铁矿床中富铁团块则显示出强烈的热液交代现象,与围岩安山质熔岩接触处普遍发育蚀变环带,包括钠长

石磁铁矿型、钠长石钾长石磁铁矿型、钾长石磁铁矿型、绿帘石磁铁矿型和石英磁铁矿型共5个类型,接触关系研究和半定量能谱分析表明不同类型的富铁团块可能是岩浆-热液连续演化的结果(Li et al., 2018)。

本文对东天山黑尖山铁矿床中5类富铁团块中的磁铁矿进行原位组分分析,从定量的角度探究富铁团块特征及其与围岩关系、富铁团块与矿石矿物的关系以及与雅满苏铁矿床富铁碎屑的对比,以期为约束东天山海相火山岩型铁矿成矿过程中岩浆演化与铁质富集的过程和联系提供依据。

2 成矿地质背景

东天山地区在大地构造位置上处于古亚洲洋南缘,是西伯利亚板块和塔里木板块的聚合地区(秦克章等,2003;王国灿等,2019)。东天山自北向南分为4个构造单元,分别是大南湖—头苏泉志留纪—早石炭世岛弧、小热泉子—梧桐窝子早石炭世弧内盆地、阿齐山—雅满苏早石炭世弧后盆地和中天山前寒武纪古陆块(图1)(秦克章等,2003; Xiao et al., 2004; Mao et al., 2005; 方维萱等,2006; Su et al., 2011)。

阿齐山—雅满苏早石炭世弧后盆地内发育众多海相火山岩铁矿床,重要的Fe-(Cu)矿床,如红云滩、百灵山、赤龙峰、黑尖山、雅满苏、沙泉子等(徐仕琪等,2011; 徐璐璐等,2014; Hou et al., 2014a,

2014b; Zhao et al., 2017, 2018; Jiang et al., 2018),构成了一个重要的海相火山岩型Fe-(Cu)成矿带。成矿带内的矿床具有相似的地质特征:(1)主要矿化时代为石炭纪;(2)围岩为海相火山岩或碎屑岩;(3)主要矿石矿物为磁铁矿;(4)矿体周围常见矽卡岩蚀变(如石榴子石和辉石);(5)与侵入体没有明显的空间联系(吴昌志等,2006; 黄小文等,2013; Huang et al., 2014; Hou et al., 2014a; Zhang et al., 2016)。

3 矿床地质特征

黑尖山铁矿床位于鄯善县城东南160 km处,构造上位于东天山阿齐山—雅满苏早石炭世弧后盆地内(图1)(秦克章等,2003),铁金属资源量1206万t, TFe平均品位43.32%,为中型铁矿床(新疆维吾尔自治区地质调查院,2003)。

矿区出露地层为上石炭统底坎尔组,其构造背景属于阿齐山—雅满苏早石炭世弧后盆地。底坎尔组自下而上可分为大致平行的3个岩性段:第一岩性段由沉凝灰岩、凝灰岩和玄武岩组成,出露于矿区的北部和东部;第二岩性段由凝灰岩、玄武安山岩和角砾凝灰岩组成,出露于矿区的西部和中部;第三岩性段为玄武安山玢岩,仅在矿区的中部和西部出露。黑尖山矿床赋矿围岩为底坎尔组的第二、三岩性段(图2)。区内岩浆活动强烈,矿床北部发育少量的石英正长斑岩、闪长玢岩和辉绿玢岩

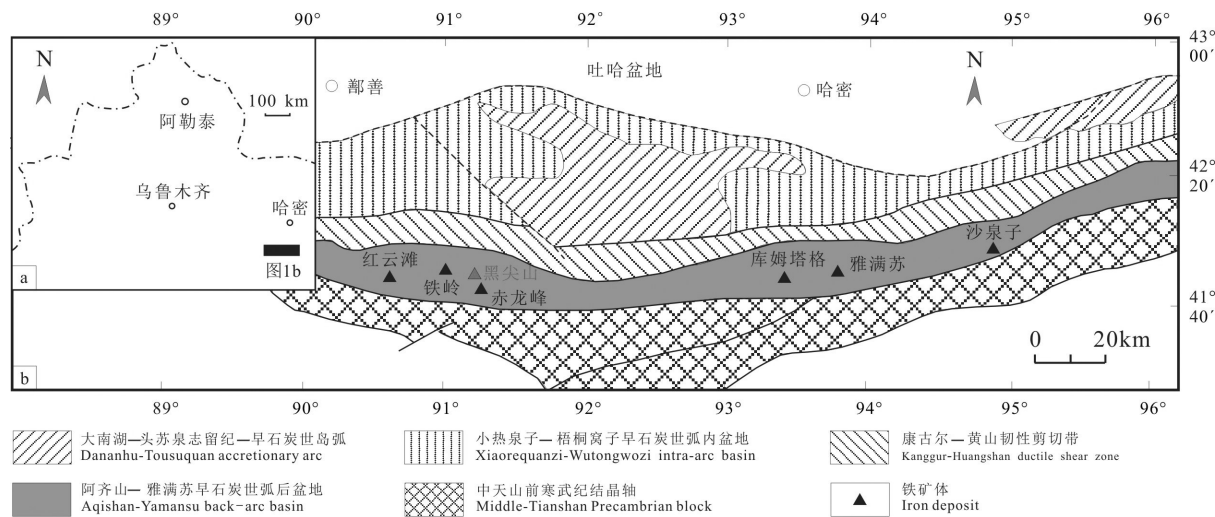


图1 东天山地区构造格架及阿齐山—雅满苏弧后盆地铁矿分布图(修改自秦克章等,2003)

Fig.1 Tectonic framework in the Eastern Tianshan orogenic belt and distribution of iron ore deposits in Aaqishan-Yamansu back-arc basin (modified from Qin Kezhang et al., 2003)

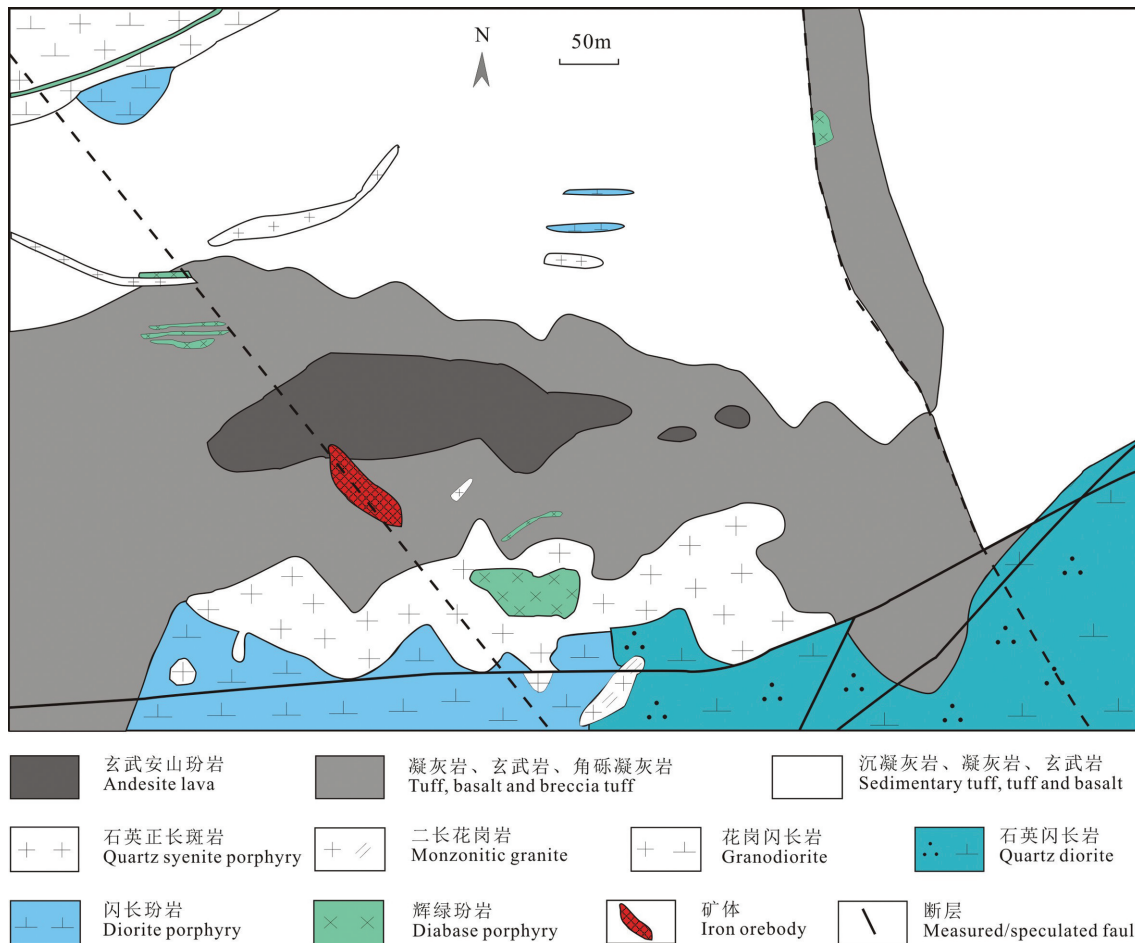


图2 黑尖山铁矿床地质图(修改自新疆维吾尔自治区地质调查院,2003;赵联党等,2017)

Fig.2 Geological map of the Heijianshan iron deposit (modified from Xinjiang Uygur Autonomous Region Geological Survey, 2003 and Zhao Liandang et al., 2017)

脉,矿床南部出露石英正长斑岩、闪长玢岩、石英闪长玢岩和少量的二长花岗岩、辉绿玢岩脉。区内晚一期断裂构造发育,其中一条断裂切穿矿体,该断裂长度5.5 km,走向310°,产状近直立(图2)。

矿体呈层状、似层状产于底坎尔组第二岩性段角砾凝灰岩、凝灰岩、安山质熔岩中,与地层产状一致。矿体平面分布范围较大,最大长度4.4 km,最大宽度2.4 km,面积为5.4 km²(图2)。矿体厚度较小,工程控制最大厚度9.59 m,平均3.22 m。矿化围岩蚀变发育,主要为绢云母化、绿泥石化、绿帘石化、硅化、碳酸盐化、孔雀石化和黄铁矿化。矿石呈浅绿色,为蚀变岩型矿石,由不同比例的磁铁矿、赤铁矿和蚀变矿物(绿泥石、石英、绿帘石、石榴石、方解石、纤闪石)组成,有时含有少量的硫化物黄铜矿、磁黄铁矿和黄铁矿等。矿石结构主要为粒状变晶

结构,矿石构造主要为网脉构造、浸染状构造和块状构造。

分布在矿体围岩火山熔岩、火山碎屑岩中富铁团块根据矿物组合可分为钠长石磁铁矿型、钠长石钾长石磁铁矿型、钾长石磁铁矿型、绿帘石磁铁矿型和石英磁铁矿型5种类型。其中钠长石磁铁矿型富铁团块具有斑状结构和杏仁构造,斑晶为钠长石,基质以钠长石和磁铁矿为主组成,其次为钾长石,其他矿物很少。富铁团块边部多为绿帘石化环边和钾长石化环边;钠长石钾长石磁铁矿型富铁团块具有斑状结构和杏仁构造,斑晶为钾长石化的钠长石和钾长石,基质以磁铁矿和钠长石、钾长石为主;钾长石磁铁矿型富铁团块主要由磁铁矿和钾长石组成,具有斑状结构和杏仁构造,围岩常见钾长石化和绿帘石化;绿帘石磁铁矿型富铁团块由绿帘

石、磁铁矿组成,具有交织结构;石英磁铁矿型富铁团块被石英交代,由石英和磁铁矿组成,但保留交织结构等原来富铁团块的结构假象。

4 样品与分析方法

根据矿物组合,富铁团块可分为钠长石磁铁矿型、钠长石钾长石磁铁矿型、钾长石磁铁矿型、绿帘石磁铁矿型和石英磁铁矿型5种类型。

钠长石磁铁矿型富铁团块以样品HJS-4,HJS-6为典型样品(图3)。HJS-4的富铁团块呈“角砾状”分布于安山质角砾熔岩中,边部有石英-绿帘石化环边,环边宽1~2 cm,含少量磁铁矿,具有由磁铁矿组成的冷凝边,内部具有斑状结构和气孔杏仁构造,斑晶为钠长石,其可被钾长石、石英交代基质为

细小磁铁矿和钠长石,有大量气孔,多为圆形,少量为不规则状,多被石英充填,个别被碳酸盐充填。HJS-6中富铁团块特征基本与HJS-4相同,内部斑状结构及气孔杏仁发育,边部也存在石英绿帘石化环边,不同的是钠长石斑晶被钾长石、石英交代的程度较大。

钠长石钾长石磁铁矿型富铁团块以样品HJS16-1为典型样品(图4),其杂乱分布于岩石中,其周围常见绿帘石晶洞。富铁团块核部由磁铁矿和钠长石组成,围岩为安山质角砾熔岩,与富铁团块界线明显,围岩多见钠长石板条以及细粒钾长石。

钾长石磁铁矿型富铁团块以样品HJS16-11为典型样品(图5),其分布于安山质角砾熔岩的裂隙中,与围岩接触边界清晰,其边部可见石英-绿帘石

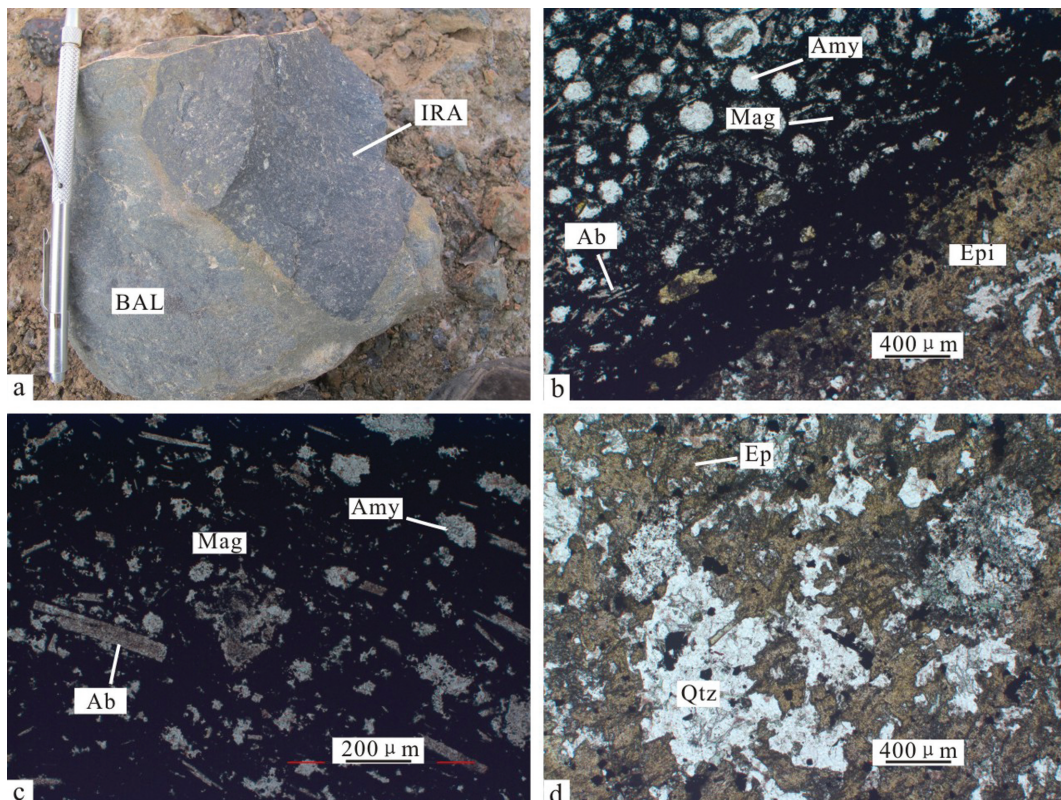


图3 钠长石磁铁矿型富铁团块手标本及显微镜下特征

a—安山岩熔岩中的富铁团块(HJS-4);b—富铁团块中的杏仁结构及其冷凝边(HJS-4);c—含有钠长石、磁铁矿、石英杏仁体的富铁团块(HJS-6);d—具有硅化和绿帘石化的安山质熔岩(HJS-6)(b, c, d均为单偏光镜下成像);Ab—钠长石;Mag—磁铁矿;Amy—杏仁体;BAL—含角砾的安山质熔岩;IRA—富铁团块;Epi—绿帘石化

Fig.3 Photographs and photomicrographs illustrating the features of the albite-magnetite type iron-rich agglomerates
a—Iron-rich agglomerates in brecciated andesite lava (HJS-4); b—Amygdaloidal structure and chilled margin of the iron-rich agglomerates (HJS-4); c—Iron-rich agglomerates composed of albite, magnetite and quartz amygdale (HJS-6); d—Andesite lava showing silicification and epidotization (HJS-6) (b, c, d are under plainlight); Ab—Albite, Mag—Magnetite; Amy—Amygdale; BAL—Brecciated andesite lava; IRA—Iron-rich agglomerates; Epi—Epidotization

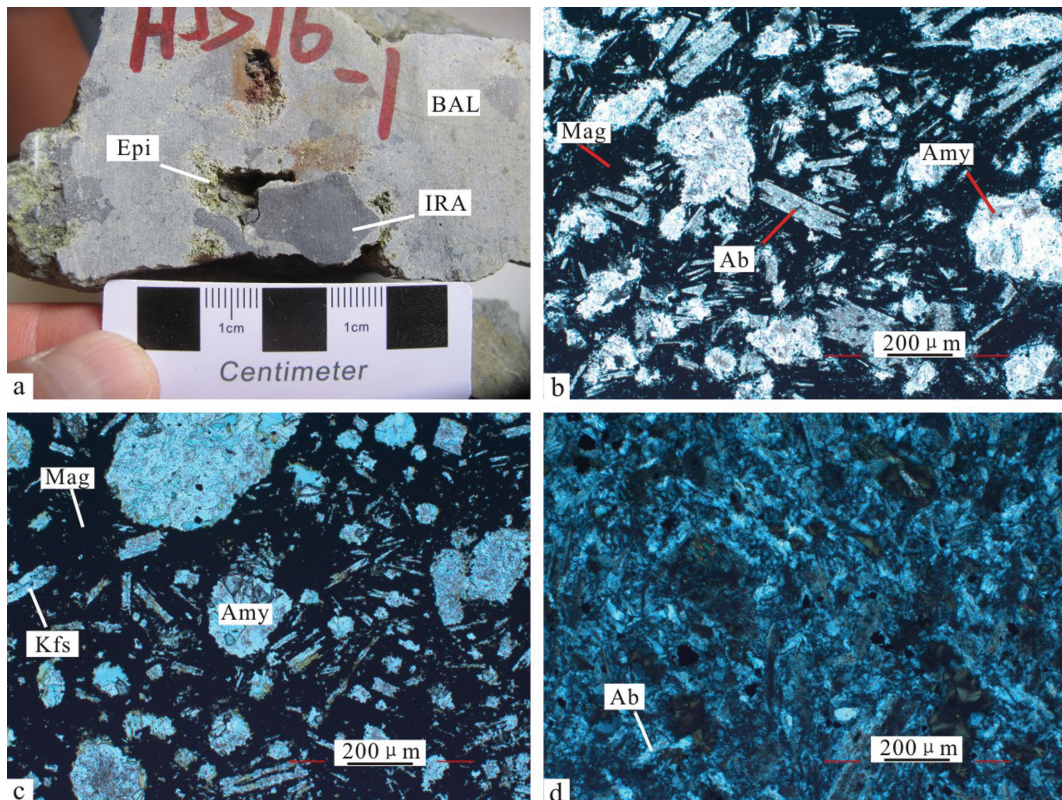


图4 钠长石钾长石磁铁矿型富铁团块手标本及显微镜下特征

a—富铁团块附近的石英—绿帘石晶洞(HJS16-1);b—含有板条状钠长石、细粒磁铁矿、石英杏仁体的富铁团块(HJS16-1);c—富铁团块(HJS16-1);d—具有玻晶交织结构的安山质熔岩(HJS16-1)(b, c为单偏光镜下成像,d为正交偏光成像);Ab—钠长石;Mag—磁铁矿;Kfs—钾长石;Amy—杏仁体;BAL—含角砾的安山熔岩;IRA—富铁团块;Epi—绿帘石化

Fig.4 Photographs and photomicrographs illustrating the features of the albite-K-feldspar-magnetite type iron-rich agglomerates a—Quartz—epidote geode near the iron-rich agglomerates (HJS16-1); b—Iron-rich agglomerates composed of lath-shaped albite, fine-grained magnetite and quartz amygdale (HJS16-1); c—Iron-rich agglomerates (HJS16-14); d—Andesite lava showing hyalopilitic structure (HJS16-1) (b, c are under plainlight); d crossed nicols); Mag—Magnetite; Kfs—K-feldspar; Amy—Amygdale; BAL—Brecciated andesite lava; IRA—Iron-rich agglomerates; Epi—Epidotization

化。富铁团块主要由磁铁矿和钾长石组成,具交织结构,主要为钾长石斑晶,钠长石少,杏仁发育,并被石英、钾长石及榍石交代。

绿帘石磁铁矿型富铁团块以样品 HJS16-9, HJS16-13 为典型样品(图 6)。样品 HJS16-9 富铁团块核部主要由细粒磁铁矿、钾长石及少量板条状钠长石组成,具斑晶、基质结构,气孔杏仁构造,杏仁可见为绿泥石。富铁团块边部绿帘石化较强,由磁铁矿、绿帘石及钠长石组成,钾长石较少。围岩为安山质角砾熔岩,由杂乱分布的板条状钠长石和分布其间的他形粒状钾长石、片状绿泥石组成,有少量磁铁矿、榍石。样品 HJS16-13 富铁团块主要由磁铁矿和钾长石组成,钠长石较少,杏仁主要为钾长石,钠长石更多在基质中。该富铁团块由未绿帘

石化和强绿帘石化两部分组成,受强烈绿帘石化的部分由磁铁矿、绿帘石及石英组成,未见钾长石及钠长石,但有较多磷灰石以及少量榍石。

石英磁铁矿型富铁团块以样品 HJS16-3 为典型样品(图 7),该富铁团块由内而外由内核、多杏仁外环以及与围岩相作用形成的冷凝边三部分组成。内核由细粒铁氧化物集合体、钾长石、碳酸盐、石英及榍石组成,无钠长石,交织结构不明显。

矿物电子探针分析以及背散射图像拍摄在中国冶金地质总局山东测试分析中心完成,所用仪器为 JEOL JXA-8230 型电子探针,实验条件为加速电压 15 kV,电流为 20 nA,束斑直径为 10 μm。K、Na 峰值积分时间为 10 s,其余元素的峰值积分时间为 20 s。

本次磁铁矿电子探针分析实验不同于常规方

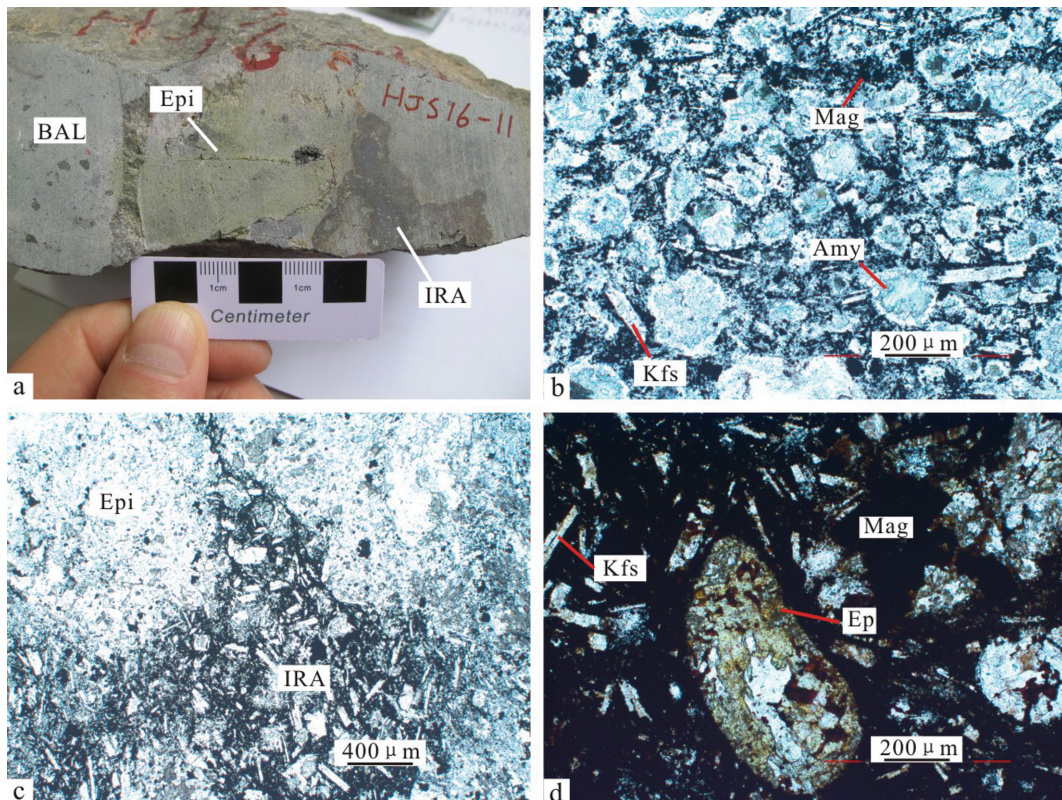


图5 钾长石磁铁矿型富铁团块手标本及显微镜下特征

a—富铁团块附近的绿帘石化边(HJS16-11);b—由绿泥石和少量钛铁矿组成的富铁团聚体中的杏仁体(HJS16-4);c—安山质熔岩中沿裂隙侵入的富铁熔体(HJS16-11);d—具有绿帘石化的富铁团块(HJS16-11)(b, c, d均为单偏光镜下成像);Mag—磁铁矿;Kfs—钾长石;Epi—绿帘石;Amy—杏仁体;BAL—含角砾的安山岩;IRA—富铁团块;Epi—绿帘石化

Fig.5 Photographs and photomicrographs illustrating the features of the K-feldspar-magnetite type iron-rich agglomerates
a—Epidotization rim of the iron-rich agglomerates (HJS16-11); b—Amygdale in the iron-rich agglomerates composed of chlorite and a trace amount of titanite (HJS16-4); c—Iron-rich melt that intruded along the fractures in the andesite lava (HJS16-11); d—Iron-rich agglomerates with epidotization (HJS16-11) (b, c, d are under plainlight); Ab—Albite, Mag—Magnetite; Kfs—K-feldspar; Ep—Epidote; Amy—Amygdale; BAL—Brecciated andesite lava; IRA—Iron-rich agglomerates; Epi—Epidotization.

法,采用差分法加入不确定的O含量,并加以ZAF矩阵校正(Love, 1993; Reed, 1993)。随后,根据测量的阳离子和添加的氧重新计算氧化物的最终含量(氧化物质量百分比),这是根据阳离子的化学计量学公式得出的。研究表明,在EPMA过程中,定义可变氧化状态阳离子的真实价态对于获得正确的测试结果至关重要(Yang et al., 2017)。因为氧化物的电子探针不能明确地测定氧的含量,所以假设一种基于阳离子价的化学计量方法,将氧元素包括在矩阵校正中。由于磁铁矿同时含有 Fe^{2+} 和 Fe^{3+} ,且非整数阳离子的价不能定义,所以采用上述方法,精确地测出磁铁矿中铁的总量,而不是铁氧化物的总量。

本次研究的实验分析点位置如图8所示,在5

种富铁团块(钠长石磁铁矿型、钾长石钾长石磁铁矿型、钾长石磁铁矿型、绿帘石磁铁矿型、石英磁铁矿型)中分别对其中的磁铁矿进行电子探针原位成分分析,有效分析共34个点,其中对除钾长石磁铁矿型富铁团块以外的其余四种富铁团块的核部和边部分别进行了分析测试,测试结果见表1。

5 分析结果

5.1 钠长石磁铁矿型

钠长石磁铁矿型富铁团块以样品HJS-4,HJS-6为典型样品进行分析。样品HJS-4富铁团块基质中细小磁铁矿的主量元素分析结果为: SiO_2 0.16%, Al_2O_3 0.04%, TFe 71.59%, MgO 0.01%, Na_2O 0.05%, V_2O_5 0.14%, TiO_2 0.05%, Cr_2O_3 0.02%等,而组成冷

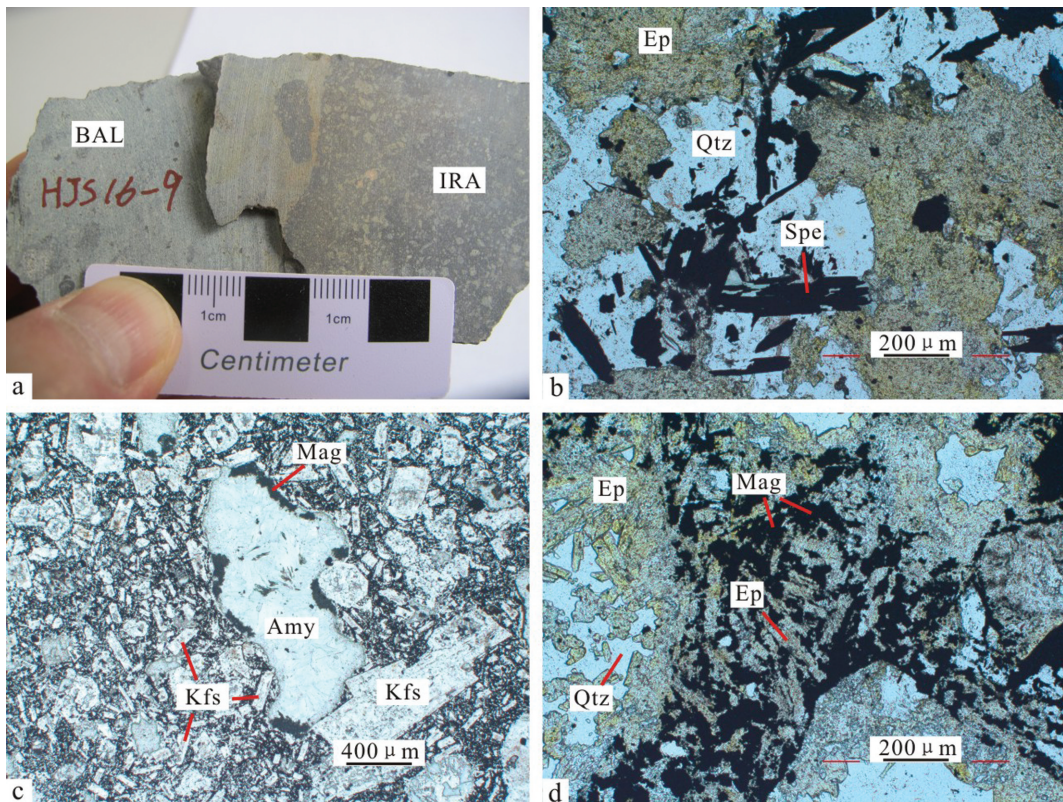


图6 绿帘石磁铁矿型富铁团块手标本及显微镜下特征

a—富铁团块(HJS16-9);b—与石英、绿帘石共生的镜铁矿(HJS16-3);c—具有斑状构造,杏仁结构的富铁团块(HJS16-9);d—被绿帘石和石英完全交代的钾长石和钠长石(HJS16-13)(b, c, d均为单偏光镜下成像);Mag—磁铁矿;Kfs—钾长石;Ep—绿帘石;Qtz—石英;Spe—镜铁矿;Amy—杏仁体;BAL—含角砾的安山熔岩;IRA—富铁团块

Fig.6 Photographs and photomicrographs illustrating the features of the epidote-magnetite type iron-rich agglomerates
 a—Iron-rich agglomerates (HJS16-9); b—Specularite platelets coexisting with epidote and quartz (HJS16-3); c—Iron-rich agglomerates showing porphyritic texture and amygdaloidal structure (HJS16-9); d—K-feldspar and albite completely replaced by epidote and quartz (HJS16-13) (b, c, d are under plainlight); Mag—Magnetite; Kfs—K-feldspar; Ep—Epidote; Qtz—Quartz; Spe—Specularite; Amy—Amygdale; BAL—Brecciated andesite lava; IRA—Iron-rich agglomerates

凝边的磁铁矿原位主量元素分析结果为: SiO_2 0.26%, Al_2O_3 0.12%, TFe 68.54%, MgO 0.03%, Na_2O 0.06%, V_2O_5 0.18%, TiO_2 0.80%, Cr_2O_3 0.04% 等。HJS-6富铁团块基质中细小磁铁矿的主量元素分析结果为: SiO_2 0.11%, Al_2O_3 0.03%, TFe 70.32%, MgO 0.01%, Na_2O 0.01%, V_2O_5 0.21%, TiO_2 0.22%, Cr_2O_3 0.04% 等。

5.2 钠长石钾长石磁铁矿型

钠长石钾长石磁铁矿型富铁团块以样品HJS16-1为典型样品进行分析。其分析结果显示富铁团块核部磁铁矿主量元素含量为: SiO_2 0.75%, Al_2O_3 0.15%, TFe 68.14%, MgO 0.07%, Na_2O 0.15%, V_2O_5 0.18%, TiO_2 0.17%, Cr_2O_3 0.03% 等; 而富铁团块边部的磁铁矿主量元素含量为: SiO_2 0.85%,

Al_2O_3 0.12%, TFe 66.73%, MgO 0.05%, Na_2O 0.12%, V_2O_5 0.26%, TiO_2 0.15%, Cr_2O_3 0.01% 等。

5.3 钾长石磁铁矿型

钾长石磁铁矿型富铁团块以样品HJS16-11为典型进行分析。样品HJS16-11中富铁团块磁铁矿主量元素含量为: SiO_2 0.19%, Al_2O_3 0.07%, TFe 68.64%, MgO 0.02%, Na_2O 0.02%, V_2O_5 0.22%, TiO_2 0.07%, Cr_2O_3 0.01% 等。

5.4 绿帘石磁铁矿型

绿帘石磁铁矿型富铁团块以样品HJS16-9、HJS16-13为典型进行分析。样品HJS16-9富铁团块磁铁矿主量元素含量为: SiO_2 0.26%, Al_2O_3 0.05%, TFe 67.77%, MgO 0.01%, Na_2O 0.09%, V_2O_5 0.19%, TiO_2 0.02%, Cr_2O_3 0.04% 等。样品HJS16-13

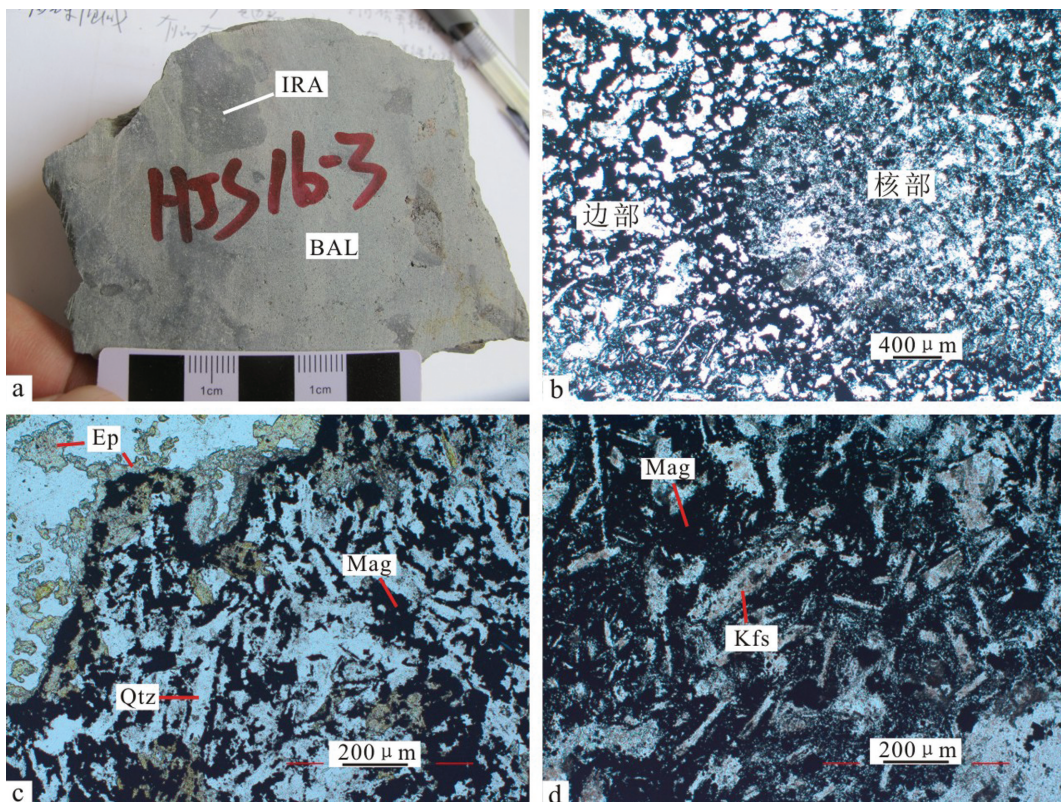


图7 石英磁铁矿型富铁团块手标本及显微镜下特征

a—富铁团块(HJS16-3);b—富铁团块的核部和边部(HJS16-3);c—保留玻晶交织结构的被石英交代的板条状长石(HJS16-3);d—冷凝边(HJS16-3)(b, c, d均为单偏光镜下成像);Mag—磁铁矿;Kfs—钾长石;Ep—绿帘石;Qtz—石英;BAL—含角砾的安山熔岩;IRA—富铁团块

Fig. 7 Photographs and photomicrographs illustrating the features of the quartz-magnetite type iron-rich agglomerates
a—Iron-rich agglomerates (HJS16-3); b—Core and rim of iron-rich agglomerates (HJS16-3); c—Lath-shaped feldspar replaced by quartz with hyalopilitic structure retained (HJS16-3); d—Chilled margin (HJS16-3) (b, c, d are under plainlight); Mag—Magnetite; Kfs—K-feldspar; Ep—Epidote; Qtz—Quartz; BAL—Brecciated andesite lava; IRA—Iron-rich agglomerates

富铁团块电子探针分析结果显示,未绿帘石化的富铁团块磁铁矿主量元素含量为: SiO_2 0.07%, Al_2O_3 0.03%, TFe 67.07%, MgO 0.02%, Na_2O 0.03%, V_2O_5 0.06%, TiO_2 0.03%, Cr_2O_3 0.01%等;受强烈绿帘石化的富铁团块磁铁矿主量元素含量为: SiO_2 0.38%, Al_2O_3 0.06%, TFe 69.28%, MgO 0.01%, Na_2O 0.04%, V_2O_5 0.15%, TiO_2 0.05%, Cr_2O_3 0.02%等。

5.5 石英磁铁矿型

石英磁铁矿型富铁团块以样品HJS16-3为典型样品进行分析。样品HJS16-3富铁团块内核中铁氧化物集合体主量元素含量为: SiO_2 0.77%, Al_2O_3 0.22%, TFe 65.60%, MgO 0.11%, Na_2O 0.11%, V_2O_5 0.19%, TiO_2 0.07%, Cr_2O_3 0.07%等。富铁团块多杏仁外环主要由磁铁矿、钾长石、钠长石和石英组成,不规则气孔杏仁发育,磁铁矿主量元素含量

为: SiO_2 0.29%, Al_2O_3 0.11%, TFe 64.70%, MgO 0.01%, Na_2O 0.10%, V_2O_5 0.29%, TiO_2 0.16%, Cr_2O_3 0.02%等。

6 讨 论

6.1 富铁团块与铁成矿的关系

富铁团块是中基性熔浆沿角砾熔岩的裂隙侵入经过冷凝结晶形成的(Li et al., 2018),这一系列中性富碱的岩浆活动为黑尖山铁矿的形成提供了有利的条件。将未蚀变围岩与硅化绿帘石化后的围岩成分对比,发现经过蚀变的原岩发生Ca、Fe带入,Na、K带出,这与矽卡岩矿化特征相似(Li et al., 2018),说明黑尖山铁矿与其他东天山海相火山岩型铁矿主要成矿阶段一致。

从5种类型的富铁团块内磁铁矿电子探针成分

表1 黑尖山铁矿床富铁团块磁铁矿电子探针测试成分(%)

Table 1 Major element analyses (EMPA) for magnetite from iron-rich agglomerates in the Heijianshan iron deposit(%)

样品号	Na ₂ O	CaO	SiO ₂	NiO	MgO	Al ₂ O ₃	MnO	Cr ₂ O ₃	V ₂ O ₅	TiO ₂	Total	TFe
HJS-4core-1	0.043	0.000	0.178	0.006	0.003	0.042	0.004	0.016	0.127	0.037	0.456	71.53
HJS-4core-2	0.049	0.000	0.139	0.000	0.000	0.030	0.000	0.023	0.148	0.070	0.459	71.65
HJS-4circle-1	0.177	0.035	0.390	0.027	0.087	0.310	0.012	0.026	0.153	0.083	1.299	68.07
HJS-4circle-2	0.071	0.000	0.268	0.000	0.037	0.161	0.000	0.040	0.109	1.123	1.808	67.97
HJS-4circle-3	0.000	0.003	0.191	0.000	0.002	0.006	0.000	0.054	0.216	1.000	1.471	70.62
HJS-4circle-4	0.006	0.000	0.178	0.065	0.000	0.011	0.013	0.058	0.228	1.007	1.565	67.51
HJS-6-1	0.003	0.000	0.088	0.029	0.000	0.026	0.006	0.034	0.221	0.233	0.641	70.13
HJS-6-2	0.000	0.108	0.139	0.000	0.020	0.030	0.017	0.044	0.205	0.200	0.763	70.52
HJS16-1core-1	0.075	0.041	0.174	0.057	0.043	0.049	0.000	0.024	0.146	0.132	0.741	67.12
HJS16-1core-2	0.267	0.105	2.211	0.000	0.100	0.408	0.000	0.019	0.193	0.040	3.343	67.28
HJS16-1core-3	0.209	0.038	0.388	0.000	0.110	0.094	0.036	0.065	0.159	0.215	1.313	68.11
HJS16-1core-4	0.065	0.000	0.214	0.000	0.020	0.038	0.039	0.012	0.218	0.285	0.891	70.03
HJS16-1circle-1	0.088	0.000	0.216	0.000	0.027	0.036	0.000	0.000	0.252	0.122	0.740	67.01
HJS16-1circle-2	0.143	0.023	1.478	0.007	0.063	0.197	0.000	0.004	0.265	0.183	2.363	66.44
HJS16-11-1	0.007	0.000	0.148	0.050	0.010	0.015	0.010	0.000	0.193	0.053	0.486	69.62
HJS16-11-2	0.019	0.000	0.152	0.000	0.030	0.159	0.001	0.000	0.337	0.083	0.782	69.59
HJS16-11-3	0.000	0.000	0.276	0.043	0.008	0.042	0.023	0.026	0.175	0.068	0.662	68.03
HJS16-11-4	0.032	0.000	0.191	0.039	0.032	0.051	0.044	0.008	0.182	0.083	0.662	67.31
HJS16-9-1	0.049	0.091	0.313	0.022	0.020	0.064	0.000	0.057	0.186	0.015	0.851	67.79
HJS16-9-2	0.139	0.066	0.336	0.000	0.005	0.076	0.000	0.051	0.186	0.018	0.877	67.48
HJS16-9-3	0.070	0.032	0.120	0.027	0.023	0.015	0.022	0.000	0.200	0.017	0.525	68.04
HJS16-13core-1	0.024	0.008	0.124	0.000	0.037	0.015	0.025	0.009	0.057	0.000	0.299	66.92
HJS16-13core-2	0.068	0.000	0.045	0.000	0.000	0.070	0.000	0.013	0.020	0.048	0.264	67.41
HJS16-13core-3	0.003	0.000	0.064	0.000	0.000	0.011	0.000	0.000	0.096	0.033	0.208	67.19
HJS16-13core-4	0.008	0.000	0.047	0.000	0.030	0.011	0.000	0.012	0.070	0.025	0.204	66.76
HJS16-13circle-1	0.038	0.000	0.619	0.000	0.008	0.125	0.000	0.043	0.159	0.053	1.045	69.45
HJS16-13circle-2	0.038	0.000	0.116	0.000	0.017	0.013	0.001	0.004	0.139	0.032	0.359	69.12
HJS16-13circle-3	0.040	0.014	0.214	0.000	0.012	0.042	0.014	0.022	0.143	0.072	0.572	69.26
HJS16-3core-1	0.082	0.106	0.827	0.000	0.067	0.219	0.000	0.110	0.189	0.158	1.759	65.00
HJS16-3core-2	0.111	0.000	1.011	0.022	0.230	0.329	0.041	0.035	0.212	0.017	2.008	65.79
HJS16-3core-3	0.129	0.036	0.471	0.017	0.027	0.125	0.000	0.053	0.166	0.025	1.049	66.00
HJS16-3circle-1	0.153	0.001	0.409	0.034	0.030	0.096	0.000	0.024	0.175	0.037	0.960	64.35
HJS16-3circle-2	0.051	0.000	0.324	0.000	0.003	0.106	0.000	0.019	0.298	0.240	1.041	65.58
HJS16-3circle-3	0.083	0.000	0.144	0.015	0.000	0.111	0.000	0.026	0.401	0.197	0.977	64.17

蛛网图(图9)中可以看出,5类富铁团块内磁铁矿的大体成分相差不大,只有Ti、Ca、K的成分有所差异:钠长石磁铁矿型具有最高的Ti含量,较低的Ca、K含量;钠长石钾长石磁铁矿型和钾长石磁铁矿型的Ti、Ca、K含量均相对较高;绿帘石磁铁矿型和石英磁铁矿型均具有较低的Ti、Ca含量,但绿帘石磁铁矿型K含量较低,石英磁铁矿型K含量较高。与各类型铁矿床中典型磁铁矿样品对比可以发现钠长石磁铁矿型富铁团块内磁铁矿的各元素成分分布

特征与IOCG型铁矿较为相似;钠长石钾长石磁铁矿型和钾长石磁铁矿型富铁团块内磁铁矿的各元素成分分布特征与Kiruna型铁矿最为接近,而绿帘石磁铁矿型和石英磁铁矿型富铁团块内磁铁矿的各元素成分分布特征则最接近矽卡岩型铁矿。相关研究证实钛氧化物在地质流体中的溶解度与温度密切相关,在低-中温条件下,钛氧化物在伴生流体中的溶解度较低,限制了钛的流动性(Van Baalen, 1993),并且前人研究指出热液成因的磁铁矿相较

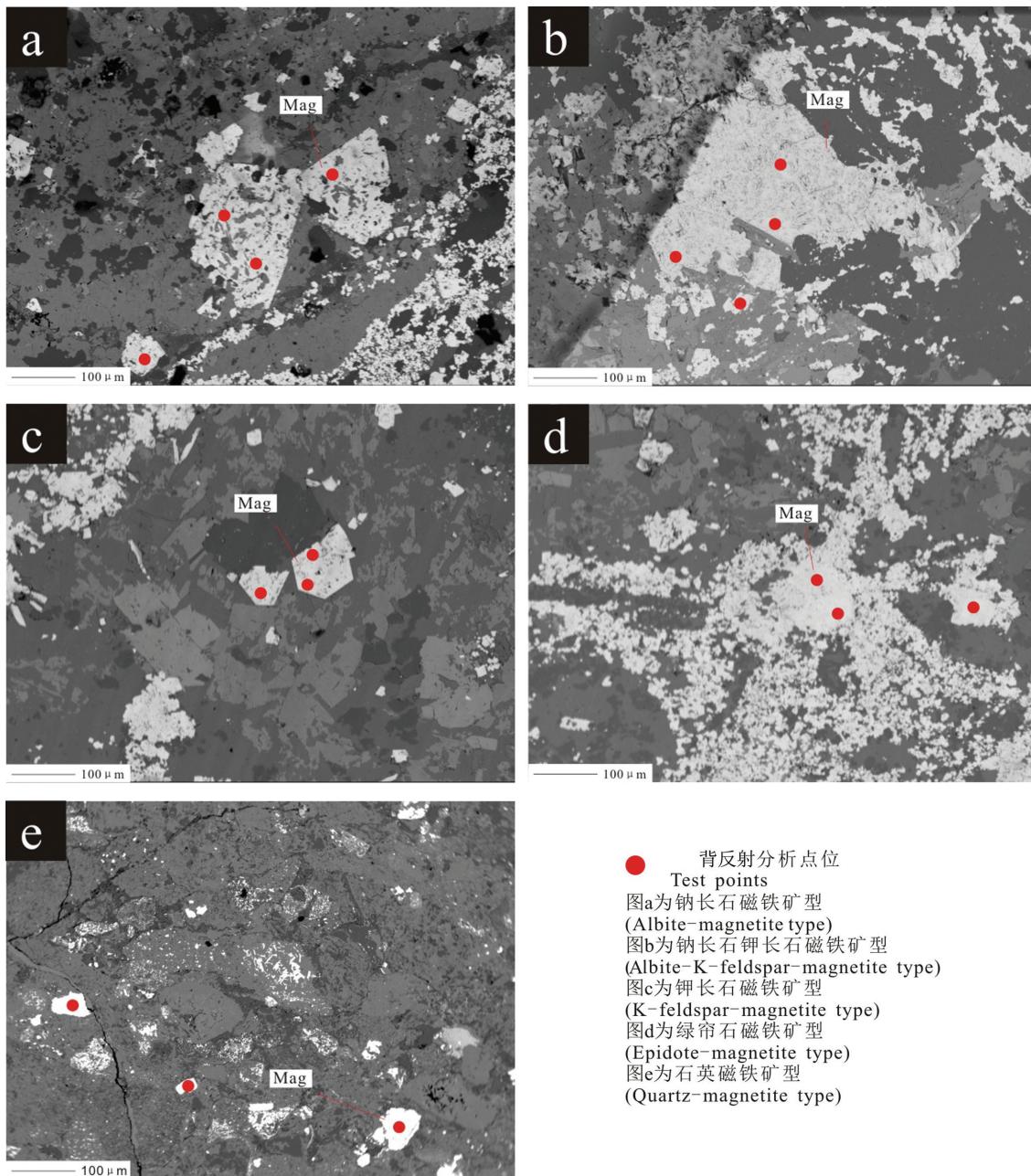


图8 黑尖山矿床富铁团块电子探针分析特征(背散射显微成像)

Fig.8 Characteristics of iron-rich agglomerates in the Heijiashan deposit by electron microprobe analysis (backscatter microscopic imaging)

岩浆成因的磁铁矿具有较低的Ti、V含量(Nadol et al., 2014),对5类磁铁矿中Ti含量进行对比研究,说明钠长石磁铁矿型富铁团块为岩浆活动产物;钠长石钾长石磁铁矿型和钾长石磁铁矿型富铁团块为岩浆-热液过渡的产物;而绿帘石磁铁矿型和石英磁铁矿型富铁团块则可能为热液作用的产物。Li et al. (2018)根据各类型富铁团块整体的成分特征、

矿物组成以及各矿物相互作用的结构特点,认为5类富铁团块是岩浆-热液过程中不同阶段的产物:钠长石磁铁矿型富铁团块可能是最早由残余富铁矿浆结晶而成,钠长石钾长石磁铁矿型和钾长石磁铁矿型富铁团块在岩浆-热液过渡的阶段形成,绿帘石磁铁矿型和石英磁铁矿型富铁团块则完全是热液交代的产物,这一结论与本文的上述推论相一致。

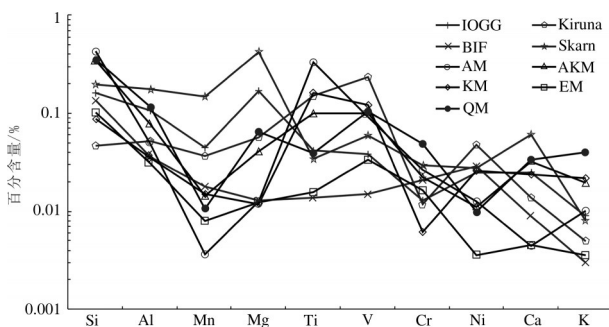


图9 富铁团块内磁铁矿主量元素成分蛛网图
IOCG, Kiruna, BIF, Skarn 数据来自 Dupuis and Beaudoin (2011);
AM—钠长石磁铁矿型; AKM—钠长石钾长石磁铁矿型; KM—钾
长石磁铁矿型; EM—绿帘石磁铁矿型; QM—石英磁铁矿型

Fig. 9 Multi-element diagram for the magnetite of iron-rich
agglomerates in the Heijiashan deposit
IOCG, Kiruna, BIF, Skarn from Dupuis and Beaudoin (2011); AM-
Albite-magnetite type; AKM-Albite-K-feldspar-magnetite type;
KM-K-feldspar-magnetite type; EM-Epidote-magnetite type;
QM-Quartz-magnetite type

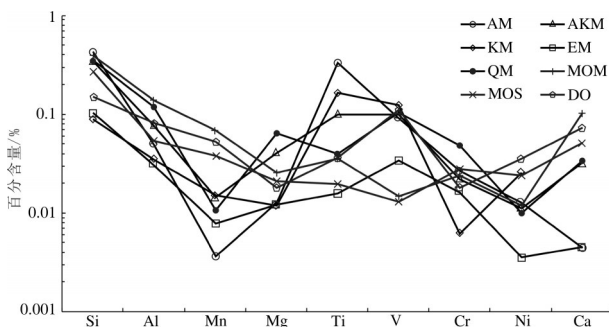


图10 富铁团块内磁铁矿与黑尖山矿床磁铁矿成分对比
黑尖山磁铁矿成分数据来自 Zhao et al. (2016); AM—钠长石磁铁矿
型; AKM—钠长石钾长石磁铁矿型; KM—钾长石磁铁矿型; EM—
绿帘石磁铁矿型; QM—石英磁铁矿型; MOM—含假象磁铁矿的块
状矿石; MOS—含硫化物的块状矿石; DO—浸染状矿石

Fig. 10 Comparison of magnetite compositions between
magnetite in iron-rich agglomerates and ore in the
Heijiashan deposit

Comparison of magnetite compositions in Heijiashan deposit after
Zhao et al. (2016); AM-Albite-magnetite type; AKM-Albite-K-
feldspar-magnetite type; KM-K-feldspar-magnetite type; EM-
Epidote-magnetite type; QM-Quartz-magnetite type; MOM-
Massive ore with mushketovite; MOS-Massive ore with sulfides;
DO-Disseminated ore

为了进一步探究富铁团块与铁成矿的关系,本文将富铁团块内磁铁矿与黑尖山矿石矿物的成分进行对比,如图10,从整体上观察发现矿石矿物除Fe外的成分含量均低于富铁团块,说明矿石矿物的

Fe更加富集,可能经过了晚期叠加的热液作用;将含假象磁铁矿的块状矿石(MOM)、含硫化物的块状矿石(MOS)、浸染状矿石(DO)与各类型富铁团块逐一对比发现,绿帘石磁铁矿型和石英磁铁矿型富铁团块的成分变化趋势与矿石矿物中磁铁矿的成分变化趋势最为相似,Zhao et al. (2016)认为黑尖山铁矿床的磁铁矿是热液成因,说明绿帘石磁铁矿型和石英磁铁矿型富铁团块是热液作用较为完全的产物,证明了上述认为绿帘石磁铁矿型和石英磁铁矿型富铁团块是残余富铁矿浆结晶且受热液完全交代产物这一推论的正确性。

6.2 东天山海相火山岩型铁矿富铁团块特征

东天山作为重要的海相火山岩型铁矿成矿区之一,主要分布于康古尔、雅满苏、阿齐山三大东西走向的断裂之间。雅满苏弧后盆地有众多海相火山岩铁矿,位于阿齐山—雅满苏断裂,其间高品位铁矿床均与海相火山岩相关,例如雅满苏、沙泉子、黑尖山、百灵山、骆驼峰等矿床。Li et al. (2015)在东天山雅满苏铁矿区矿体底板及下盘的火山角砾岩、沉火山角砾岩及熔结凝灰岩中发现了大量富铁岩浆岩碎屑,可划分为更长石铁氧化物型、更长石钠长石铁氧化物型、钠长石铁氧化物型、钠长石钾长石铁氧化物型和钾长石铁氧化物型5种类型。这与黑尖山矿体围岩安山质熔岩中发育的大量富铁团块有许多相似的特征,例如:两者内部均具有明显的斑晶-基质结构、交织结构和气孔杏仁构造,基质主体均是磁铁矿和长石,斑晶均为长石等等。

为了进一步了解两个矿床富铁组构的异同,探究东天山海相火山岩型铁矿区域成矿规律,本文将黑尖山铁矿床富铁团块主体部分的磁铁矿和雅满苏铁矿床富铁碎屑中的磁铁矿的电子探针原位分析数据对比(图11),雅满苏铁矿床富铁碎屑中的磁铁矿Fe含量为62.35%~69.27%,黑尖山铁矿床富铁团块主体部分的磁铁矿Fe含量为65.00%~71.65%,区间差别不大,可能是两个铁矿的富铁组构都来自残余富铁矿浆;黑尖山铁矿床富铁团块Fe含量、Si含量整体大于雅满苏铁矿床富铁碎屑,而黑尖山铁矿床富铁团块Al含量、Ti含量、V含量整体小于雅满苏铁矿床富铁碎屑,这说明黑尖山富铁团块在较低的温度下演化,期间发生了绿帘石化、硅化等热液活动,较多的Fe含量有利于热液交代使Fe迁移

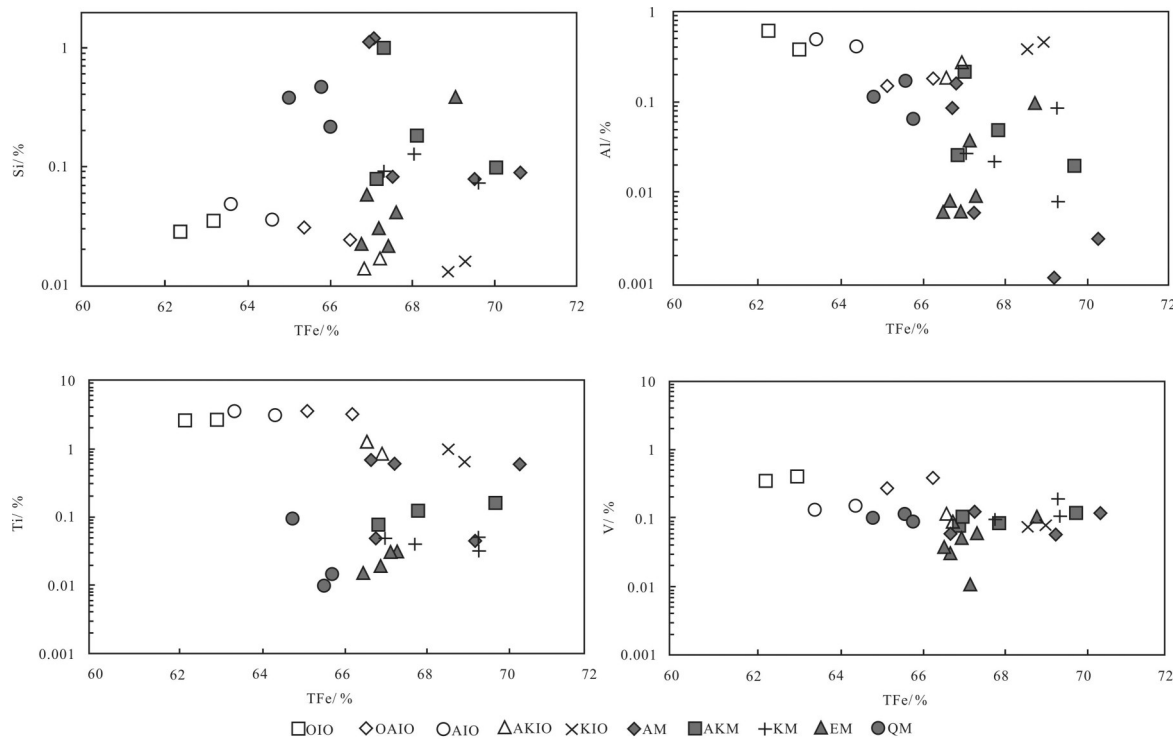


图11 黑尖山铁矿床富铁团块核部磁铁矿和雅满苏铁矿床富铁碎屑中的磁铁矿成分对比

雅满苏铁矿床富铁碎屑中的磁铁矿成分来自 Li et al. (2015); AM—钠长石磁铁矿型; AKM—钠长石钾长石磁铁矿型; KM—钾长石磁铁矿型; EM—绿帘石磁铁矿型; QM—石英磁铁矿型; OIO—更长石铁氧化物型; OAIO—更长石钠长石铁氧化物型; AIO—钠长石铁氧化物型; AKIO—钠长石钾长石铁氧化物型; KIO—钾长石铁氧化物型

Fig. 11 Comparison of magnetite compositions in iron-rich agglomerates of the Heijianshan iron deposit and in iron-rich fragments of the Yamansu iron deposit

Comparison of magnetite compositions in iron-rich fragments of the Yamansu iron deposit after Li et al. (2015); AM—Albite-magnetite type, AKM—Albite-K-feldspar-magnetite type; KM—K-feldspar-magnetite type; EM—Epidote-magnetite type; QM—Quartz-magnetite type; OIO—Oligoclase-iron oxide type; OAIO—Oligoclase-albite-iron oxide type; AIO—Albite-iron oxide type; AKIO—Albite-K-feldspar-iron oxide type; KIO—K-feldspar-iron oxide type

富集;两者的Si含量、Al含量与Fe含量均为负相关,雅满苏铁矿床富铁碎屑的Ti、V含量与Fe含量相关性较差,而黑尖山铁矿床富铁团块的Ti含量与Fe含量具有明显的正相关性,这说明黑尖山铁矿床富铁团块经过热液作用,在演化过程中,残余岩浆结晶与热液活动同时进行,使其温度降低,Fe被带出,在热液交代处进一步富集,而雅满苏铁矿床富铁碎屑的样品没有显示出热液活动的特征,始终为原始的残余岩浆。综上所述,黑尖山铁矿床富铁团块主体部分的磁铁矿和雅满苏铁矿床富铁碎屑中的磁铁矿成因相似,均为岩浆分离结晶晚期,由富含挥发分的残余富铁岩浆(矿浆)贯入形成,但黑尖山铁矿床富铁团块主体部分的磁铁矿经历了热液交代,温度降低,使得Fe等元素成分迁移,而雅满苏铁矿床富铁碎屑中的磁铁矿热液作用特征不明显,

仍表现为原始残余岩浆的特征。

7 结 论

综上所述,黑尖山矿床富铁团块内的磁铁矿成分特征主要意义是指示黑尖山铁矿床的岩浆-热液成矿过程以及经历了岩浆-热液过渡的成矿环境。具体表现如下:

(1)黑尖山矿床富铁团块内的磁铁矿Fe含量均大于相对应蚀变环边的磁铁矿Fe含量,且成分相差不大,说明在热液交代过程中富铁团块中Fe可能同时发生原始富铁残浆加入和Fe被热液交代至围岩形成蚀变环边,因此热液活动与富铁岩浆结晶分异同期发生。

(2)根据5类磁铁矿Ti含量的对比,发现钠长石磁铁矿型富铁团块为岩浆活动产物;钠长石钾长石

磁铁矿型和钾长石磁铁矿型富铁团块为岩浆-热液过渡的产物;而绿帘石磁铁矿型和石英磁铁矿型富铁团块则可能为热液作用的产物。

(3)绿帘石磁铁矿型和石英磁铁矿型富铁团块的成分变化趋势与矿石矿物中磁铁矿的成分变化趋势最为相似,且黑尖山铁矿床为热液成因,所以绿帘石磁铁矿型和石英磁铁矿型富铁团块是残余富铁矿浆结晶且受热液完全交代产物,对矿床成因的探究有指示意义。

(4)黑尖山铁矿床富铁团块主体部分的磁铁矿和雅满苏铁矿床富铁碎屑中的磁铁矿成因相似,均为岩浆分离结晶晚期,由富含挥发分的残余富铁岩浆(矿浆)贯入形成的。但黑尖山铁矿床富铁团块主体部分的磁铁矿经历了热液交代,温度降低,使得Fe等元素成分迁移,而雅满苏铁矿床富铁碎屑中的磁铁矿热液作用特征不明显,仍表现为原始残余岩浆的特征。

Reference

- Barton M D. 2014. Iron Oxide (- Cu- Au- REE- P- Ag- U- Co) Systems[J]. University of Arizona. Chapter 515-541.
- Charlier B, Grove T L. 2012. Experiments on liquid immiscibility along tholeiitic liquid lines of descent[J]. Contributions to Mineralogy and Petrology, 164: 27-44.
- Chen Jie, Duan Shigang, Zhang Zuoheng, Luo Gang, Jiang Zongsheng, Luo Wenjuan, Wang Dachuan, Zheng Renqiao. 2014. Geology, mineral chemistry and sulfur isotope geochemistry of the Shikebutai iron deposit in West Tianshan Mountains, Xinjiang: Constraints on genesis of the deposit[J]. Geology in China, 41(6): 1833-1852(in Chinese with English abstract).
- Dare S A S, Barnes S, Beaudoin G. 2015. Did the massive magnetite "lava flows" of El Laco (Chile) form by magmatic or hydrothermal processes? New constraints from magnetite composition by LA-ICP-MS[J]. Mineralium Deposita, 50: 607-617.
- Ding Jianhua, Li Houmin, Li Lixing, Chen Jing and Deng Gang. 2017. Geological and geochemical features and genetic significant of carbonatite in Yamasu iron deposit, Xinjiang[J]. Mineral Deposits, 36(1): 219-236(in Chinese with English abstract).
- Duan Chao, Li Yanhe, Mao Jingwen, Hou Kejun, Yuan Shunda. 2012. Zircon trace element characteristics of intrusions in the Washan iron deposit of Ningwu volcanic basin and their geological significance[J]. Geology in China, 39(6): 1874- 1884(in Chinese with English abstract).
- Duan Shigang, Zhang Zuoheng, Wei Mengyuan, Tian Jingquan, Jiang Zongsheng, Li Fengming, Zhao Jun, Wang Houfang. 2014. Geochemistry and zircon U-Pb geochronology of the diorite associated with the Wuling iron deposit in Western Tianshan Mountains, Xinjiang[J]. Geology in China, 41(6): 1757- 1770(in Chinese with English abstract).
- Duchesne J C, Shumlyanskyy L, Charlier B. 2006. The Fedorivka layered intrusion (Korosten Pluton, Ukraine): an example of highly differentiated ferrobasaltic evolution[J]. Lithos, 89: 353-376.
- Dupuis C, Beaudoin G. 2011. Discriminant diagrams for iron oxide trace element fingerprinting of mineral deposit types[J]. Mineralium Deposita, 46: 319-335.
- Fang Weixuan, Huang Zhuanying, Tang Hongfeng, Gao Zhenquan. 2006. Lithofacies, geological and geochemical characteristics and tectonic setting of Late Carboniferous volcanic-sedimentary rocks in the Kumtag-Shaquanzi area, east Tianshan[J]. Geology in China, 33(3): 529-544(in Chinese with English abstract).
- Feng Jing, Xu Shiqi, Tian Jiangtao, Yang Zaifeng, Gao Yongfeng. 2009. Study on metallogenic regularity of marine volcanic-type iron ore of east Tianshan of Xinjiang and methods discuss[J]. Xinjiang Geology, 27(4): 330-336 (in Chinese with English abstract).
- Fenner C N. 1929. The crystallization of basalt [J]. American Journal of Science, 18: 225-253.
- Frietsch R. 1978. On the magmatic origin of iron ores of the Kiruna type [J]. Economic Geology, 73 (4): 478-485.
- Gleason J D, Marikos M A, Barton M D, Johnson D A. 2000. Neodymium isotopic study of rare earth element sources (Fe-P-REE) systems and mobility in hydrothermal Fe oxide[J]. Geochimica et Cosmochimica Acta, 64: 1059-1068.
- Hildebrand R S. 1986. Kiruna-type deposits; their origin and relationship to intermediate subvolcanic plutons in the Great Bear magmatic zone, Northwest Canada[J]. Economic Geology, 81:640-659.
- Hou Tong, Zhang Zhaochong, Du Yangsong. 2010. Deep ore magma-hydrothermal system of Zhonggu ore field in southern part of Ningwu Basin[J]. Earth Science Frontiers, 17(1): 186- 194(in Chinese with English abstract).
- Hou Tong, Zhang Zhaochong, Pirajno F, Santosh M, Encarnacion J, Liu Junlai, Zhao Zhidan, Zhang Lijian. 2014a. Geology, tectonic settings and iron ore metallogenesis associated with submarine volcanism in China: An overview[J]. Ore Geol. Rev., 57: 498-517.
- Hou Tong, Zhang Zhaochong, Santosh M, Encarnacion J, Zhu Jiang, Luo Wenjuan. 2014b. Geochronology and geochemistry of submarine volcanic rocks in the Yamansu iron deposit, Eastern Tianshan Mountains, NW China: Constraints on the metallogenesis[J]. Ore Geol. Rev., 56: 487-502.
- Huang Xiaowen, Qi Liang, Meng Yumiao. 2013. Trace element and REE geochemistry of minerals from Heifengshan, Shuangfengshan and Shaquanzi (Cu-Fe) deposits, eastern Tianshan Mountains[J]. Mineral Deposits, 32(6): 1188- 1210(in Chinese with English abstract).
- Huang Xiaowen, Qi Liang, Wang Yichang, Liu Yingying. 2014. Re-

- Os dating of magnetite from the Shaquanzi Fe–Cu deposit, eastern Tianshan, NW China[J]. *Sci. China (Earth Sci.)*, 57: 267–277.
- Jang Y D, Naslund H R, McBirney A R. 2001. The differentiation trend of the Skaergaard intrusion and the timing of magnetite crystallization: Iron enrichment revisited[J]. *Earth and Planetary Science Letter*, 189: 189–196.
- Jiang Hongjun, Han Jinsheng, Chen Huayong, Zheng Yi, Zhang Weifeng, Lu Wanjian, Deng Gang, Tan Zhixiong. 2018. Hydrothermal alteration, fluid inclusions and stable isotope characteristics of the Shaquanzi Fe–Cu deposit, eastern Tianshan: implications for ore genesis and deposit type[J]. *Ore Geol. Rev.* 200: 385–400.
- Knipping J L, Bilener L D, Simon A C, Reich M, Barra F, Deditius A P, Wölle M, Heinrich C A, Holtz F, Munizaga R. 2015. Trace elements in magnetite from massive iron oxide–apatite deposits indicate a combined formation by igneous and magmatic–hydrothermal processes [J]. *Geochimica et Cosmochimica Acta*, 171: 15–38.
- Li Houmin, Wang DENGHONG, Li Lixing, Chen Jing, Yang Xiuqing, Liu Mingjun. 2012. Metallogeny of iron deposits and resource potential of major iron mineralogic units in China[J]. *Geology in China*, 39 (3): 559–580(in Chinese with English abstract).
- Li Houmin, Li Lixing, Yang Xiuqing, Cheng Yanbo. 2015a. Types and geological characteristics of iron deposits in China[J]. *Journal of Asian Earth Sciences*, 103: 2–22.
- Li Houmin, Ding Jianhua, Zhang Zhaochong, Li Lixing, Chen Jing, Yao Tong. 2015b. Iron– rich fragments in the Yamansu iron deposit, Xinjiang, NW China: Constraints on metallogenesis[J]. *Journal of Asian Earth Sciences*, 113: 1068–1081.
- Li Houmin, Li Lixing, Ding Jianhua, Li Yanhe, Song Zhe, Meng Jie, Ma Yubo. 2018. Occurrence of the Iron– rich melt in the Hejianshan Iron deposit, Eastern Tianshan, NW China: Insights into the origin of volcanic rock– hosted Iron deposits[J]. *Acta Geologica Sinica (English Edition)*, 92(2): 666–681.
- Li Xiaolinbin, Gong Xiaoping, Ma Huadong, Han Qiong, Song Xianglong, Xie Lei, Feng Jun, Wang Jianshe. 2014. Geochemical characteristics and petrogenic age of volcanic rocks in the Shikebutai iron deposit of West Tianshan Mountains[J]. *Geology in China*, 41(6): 1791–1804(in Chinese with English abstract).
- Love G. 1993 X– ray absorption correction[C]//Scott V D, Love G (eds.). Quantitative Electron– Probe Microanalysis. Ellis Horwood Ltd Press (Chichester, UK), 163–192.
- Luo Ting, Liao Qun'an, Chen Jiping, Zhang Xionghua, Guo Dongbao, Hu Zhaochu. 2012. LA– ICP– MS zircon U– Pb dating of the volcanic rocks from Yamansu Formation in the Eastern Tianshan, and its geological significance[J]. *Earth Science—Journal of China University of Geosciences*, 37(6): 1338– 1352(in Chinese with English abstract).
- Mao Jingwen, Goldfarb R J, Wang Yitian, Hart C J, Wang Zhiliang, Yang Jianmin. 2005. Late Paleozoic base and precious metal deposits, east Tianshan, Xinjiang, China: Characteristics and geodynamic setting[J]. *Episodes*, 28: 23–35.
- Nadol P, Angerer T, Mauk J L, French D, Walshe J. 2014. The chemistry of hydrothermal magnetite: a review [J]. *Ore Geology Reviews*, 61: 1–32.
- Naslund H R. 1983. The effect of oxygen fugacity on liquid immiscibility in iron– bearing silicate melts [J]. *American Journal of Science*, 283: 1034–1059.
- Naslund H R, Henriquez F, Nystrom J O, Vivallo W, Dobbs F M. 2002. Magmatic iron ores and associated mineralization: Examples from the Chilean high Andes and coastal Cordillera[C]//Porter T M (ed.). *Hydrothermal Iron Oxide Copper– Gold and Related Deposits: A Global Perspective*: Adelaide, Australia. PGC Publishing.
- Nyström J O, Henriquez F. 1994. Magmatic features of iron ores of the Kiruna type in Chile and Sweden: Ore textures and magnetite geochemistry[J]. *Economic Geology*, 89: 820–839.
- Park C F. 1961. A magnetite “flow” in northern Chile[J]. *Economic Geology*, 56: 431–441.
- Philpotts A R. 1982. Compositions of immiscible liquids in volcanic rocks[J]. *Contributions to Mineralogy and Petrology*, 80: 201–218.
- Porter T M. 2002. *Hydrothermal Iron Oxide Copper–Gold and Related Deposits: A Global Perspective*. Australian Mineral Foundation[M]. PGC Publishing, Adelaide. 2, 153–161.
- Qin Kezhang, Peng Xiaoming, San Jinzhu, Xu Xingwang, Fang Tonghui, Wang Shulai, Yu Haifeng. 2003. Types of major ore deposits, division of metallogenic belts in Eastern Tianshan, and discrimination of potential prospects of Cu, Au, Ni mineralization[J]. *Xinjiang Geology*, 21(2): 143– 150(in Chinese with English abstract).
- Reed S J B. 1993. *Electron Microprobe Analysis*[M]. Cambridge University Press (Cambridge, UK), 260.
- Rhodes A L, Oreskes N, Sheets S. 1999. Geology and rare earth element geochemistry of magnetite deposits at El Laco, Chile[J]. *Soc. Econ. Geol. Spec. Publ.*, 7:299–332.
- Sillitoe R H, Burrows D R. 2002. New field evidence bearing on the origin of the El Laco magnetite deposit, northern Chile[J]. *Economic Geology*, 97: 1101–1109.
- Su Benxun, Qin Kezhang, Sakyi P A, Li Xianhua, Yang Yueheng, Sun He, Tang Dongmei, Liu Pingping, Xiao Qinghua, Sanjeeva P K. Malaviarachchi. 2011. U– Pb ages and Hf– O isotopes of zircons from Late Paleozoic mafic– ultramafic units in the southern Central Asian Orogenic Belt: tectonic implications and evidence for an Early–Permian mantle plume[J]. *Gondwana Res.*, 20: 516–531.
- Tornos F, Velasco F, Morata D, Barra F, Rojo M. 2011. The magmatic hydrothermal evolution of the El Laco as tracked by melt inclusions and isotope data[C]// Barra F, Reich M F T (eds.) . Proceedings of the 11th Biennial SGA Meeting. Antofagasta, Chile,

- 443–445.
- Tornos F, Velasco F, Hanchar J M. 2016. Iron oxide melts, magmatic magnetite and superheated magmatic–hydrothermal systems: The El Laco deposit, Chile[J]. *Geology*, 44(6): 427–430.
- Van Baalen M R. 1993. Titanium mobility in metamorphic systems: A review[J]. *Chemical Geology*, 110: 233–249.
- Veksler I V. 2009. Extreme iron enrichment and liquid immiscibility in mafic intrusions: Experimental evidence revisited [J]. *Lithos*, 111: 72–82.
- Velasco F, Tornos F, Hanchar J M. 2016. Immiscible iron– and silica-rich melts and magnetite geochemistry at El Laco volcano (northern Chile): Evidence for a magmatic origin for the magnetite deposits [J]. *Ore Geology Reviews*, 79: 346–366.
- Wang Dachuan, Jia Jindian, Duan Shigang, Zhang Zuoheng, Jiang Zongsheng, Chen Jie. 2014. Mineralogy and stable isotopic characteristics of the Tiemulike iron deposit in West Tianshan Mountains[J]. *Geology in China*, 41(6): 1853–1872(in Chinese with English abstract).
- Wang Guocan, Zhang Meng, Zhang Xionghua, Liao Qun'an, Wang Wei, Tian Jiming, Xuan Zeyou. 2019. Significant Paleozoic tectonic events in the northern part of the east Tianshan Mountains, Xinjiang and their implications for the evolution of CAOB: New evidence from 1: 50000 geological survey of Banfanggou and Xiaoliogou sheets[J]. *Geology in China*, 46(5): 954–976(in Chinese with English abstract).
- Wang Tiezhu, Che Linrui, Yu Jinjie, Lu Bangcheng. 2014. Electron microprobe analysis and REE geochemical characteristics of minerals from the Meishan iron deposit in Nanjing–Wuhu area, Eastern China[J]. *Geology in China*, 41(6): 1964–1985(in Chinese with English abstract).
- Williams P J, Barton M D, Johnson D A, Fontbote L, de Haller A, Mark G, Oliver N H S, Marschik R. 2005. Iron Oxide Copper–Gold Deposits: Geology, Space–time Distribution and Possible Modes of Origin[J]. *Economic Geology* 100th Anniversary Volume SEG, Denver, 371–405.
- Xiao Wenjiao, Zhang Lianchang, Qin Kezhang, Sun Shu, Li Jiliang. 2004. Paleozoic accretionary and collisional tectonics of the eastern Tianshan (China): Implications for the continental growth of central Asia[J]. *Am. J. Sci.*, 304: 370–395.
- Xinjiang Uygur Autonomous Region Geological Survey (abv. XUARGS), 2003. Report for Target Selection and Potential Resources in Caixiasan–Jintan in the Eastern Tianshan, Xinjiang[R]. 1–187 (in Chinese).
- Xu Lulu, Chai Fengmei, Li Qiang, Zeng Hong, Geng Xinxia, Xia Fang, DengGang. 2014. Geochemistry and zircon U–Pb age of volcanic rocks from the Shaquanzi Fe–Cu deposit in east Tianshan mountains and their geological significance[J]. *Geology in China*, 41(6): 1771–1790 (in Chinese with English abstract).
- Xu Shiqi, Zhao Tongyang, Feng Jing, Gao Yongfeng, Tian Jiangtao, Yang Zaifeng, Liu Dequan. 2011. Study on regional metallogenetic regularity of marine volcanic type iron ore in the east Tianshan of Xinjiang[J]. *Xinjiang Geology*, 29(2): 173–177 (in Chinese with English abstract).
- Yang Shuiyuan, Zhang Ruoxi, Jiang Shaoyong, Xie Jing. 2017. Electron Probe Microanalysis of variable oxidation state oxides: protocol and Pitfalls[J]. *Geostandards and Geoanalytical Research*.
- Zeng Hong, Chai Fengmei, Zhou Gang, Geng Xinxia, Li Qiang, Meng Qingpeng, Xu Lulu. 2014. Mineralogy of skarn and magnetite of the Yamansu iron deposit and its geological significance[J]. *Geology in China* 41(6): 1914–1928 (in Chinese with English abstract).
- Zhang Zhaochong, Hou Tong, Santosh M, Li Houmin, Li Jianwei, Zhang Zuoheng, Song Xueyan, Wang Meng. 2014. Spatio-temporal distribution and tectonic settings of the major iron deposits in China: an overview[J]. *Ore Geol. Rev.*, 57: 247–263.
- Zhang Zhaochong, Chai Fengmei, Xie Qiuhong. 2016. Highangle subduction in a thermal structure with warm mantlecool crust: formation of submarine volcanic–hosted iron deposits[J]. *Geology in China*, 43(2): 367–379 (in Chinese with English abstract).
- Zhang Zhenliang, Feng Xuanjie, Gao Yongwei, Wang Zhihua, Dong Fuchen, Tan Wenjuan. 2015. A tentative discussion on the genetic type and ore– forming process of main late Paleozoic magnetite deposits in West Tianshan Mountains, Xinjiang[J]. *Geology in China*, 42 (2): 737–758 (in Chinese with English abstract).
- Zhang Weifeng, Chen Huayong, Han Jinsheng, Zhao Liandang, Huang Jianhan, Yang Juntao, Yan Xuelu. 2016. Geochronology and geochemistry of igneous rocks in the Bailingshan area: Implications for the tectonic setting of late Paleozoic magmatism and iron skarn mineralization in the eastern Tianshan, NW China[J]. *Gondwana Res.*, 38: 40–59.
- Zhao Hongjun, Chen Xiufa, He Xuezhou, Zhang Xinyuan, Zhang Chao, Wang Liangliang, Chen Yuming, Chen Xifeng, Lu Minjie, Zhou Shangguo, Huang Feixin, Yao Chunyan, Yang Yanchen. 2018. A study of genetic type characteristics and important distribution zones of global iron deposits[J]. *Geology in China*, 45 (5): 890–919 (in Chinese with English abstract).
- Zhao Liandang, Chen Huayong, Zhang Li, Li Dengfeng, Zhang Weifeng, Wang Chengming, Yang Juntao, Yan Xuelu. 2017. Magnetite geochemistry of the Heijiashan Fe–Cu (–Au) deposit in Eastern Tianshan: Metallogenetic implications for submarine volcanic–hosted Fe–Cu deposits in NW China [J]. *Ore Geol. Rev.*, 91: 110–132.
- Zhao Liandang, Chen Huayong, Zhang Li, Li Dengfeng, Zhang Weifeng, Wang Chengming, Yang Juntao, Yan Xuelu. 2016. Magnetite geochemistry of the Heijiashan Fe–Cu (–Au) deposit in Eastern Tianshan: metallogenetic implications for submarine volcanic–hosted Fe–Cu deposits in NW China[J]. *Ore Geol. Rev.*, 100: 422–440.

Zhao Liandang, Chen Huayong, Zhang Li, Zhang Zengjie, Li Dengfeng, Zhang Weifeng, Lu Wanjian, Yang Jun and Yan Xuelu. 2017. H–O isotope characteristics and geological significance of Heijianshan Fe–Cu (–Au) deposit in eastern Tianshan, Xinjiang[J]. Mineral Deposits, 36(1): 38–56 (in Chinese with English abstract).

附中文参考文献

- 陈杰,段士刚,张作衡,罗刚,蒋宗胜,骆文娟,王大川,郑仁乔.2014.新疆西天山式可布台铁矿地质、矿物化学和S同位素特征及其对矿床成因的约束[J].中国地质,41(6):1833–1852.
- 丁建华,李厚民,李立兴,陈清,邓刚.2017.新疆雅满苏铁矿床碳酸盐岩地质地球化学特征及其对矿床成因的制约[J].矿床地质,36(1):219–236.
- 段超,李延河,毛景文,侯可军,袁顺达.2012.宁芜火山岩盆地凹山铁矿床侵入岩锆石微量元素特征及其地质意义[J].中国地质,39(6):1874–1884.
- 段士刚,张作衡,魏梦元,田敬俊,蒋宗胜,李凤鸣,赵军,王厚方.2014.新疆西天山雾岭铁矿闪长岩地球化学及锆石U–Pb年代学[J].中国地质,39(6):1757–1770.
- 方维萱,黄转盈,唐红峰,高珍权.2006.东天山库姆塔格—沙泉子晚石炭世火山—沉积岩相学地质地球化学特征与构造环境[J].中国地质,33(3):529–544.
- 冯京,徐仕琪,田江涛,杨在峰,高永峰.2009.东天山海相火山岩型铁矿成矿规律研究方法[J].新疆地质,27(4):330–336.
- 侯通,张招崇,杜杨松.2010.宁芜南段钟姑矿田的深部矿浆–热液系统[J].地学前缘,17(1):186–194.
- 黄小文,漆亮,孟郁苗.2013.东天山黑峰山、双峰山及沙泉子(铜)铁矿床的矿物微量和稀土元素地球化学特征[J].矿床地质,32(6):1188–1210.
- 李厚民,王登红,李立兴,陈靖,杨秀清,刘明军.2012.中国铁矿成矿规律及重点矿集区资源潜力分析[J].中国地质,39(3):559–580.
- 李厚民,丁建华,李立兴,姚通.2014.东天山雅满苏铁矿床矽卡岩成因及矿床成因类型[J].地质学报,88(12):2477–2489.
- 李潇林斌,弓小平,马华东,韩琼,宋相龙,谢磊,凤骏,王建设.2014.西天山式可布台铁矿火山岩地球化学特征、成岩时代厘定及其构造意义[J].中国地质,39(6):1791–1804.
- 罗婷,廖群安,陈继平,张雄华,郭东宝,胡兆初.2012.东天山雅满苏组火山岩LA–ICP–MS锆石U–Pb定年及其地质意义[J].地球科学——中国地质大学学报,37(6):1338–1352.
- 秦克章,彭晓明,三金柱,徐兴旺,方同辉,王书来,于海峰.2003.东天山主要矿床类型、成矿区带划分与成矿远景区优选[J].新疆地质,21(2):143–150.
- 王大川,贾金典,段士刚,张作衡,蒋宗胜,陈杰.2014.西天山铁木里克铁矿床矿物学及稳定同位素特征[J].中国地质,41(6):1853–1872.
- 王国灿,张孟,张雄华,廖群安,王玮,田锦明,玄泽悠.2019.东天山北部古生代重大构造事件及其对中亚造山带演化的启示:基于1:5万板房沟幅和小柳沟幅地质调查新证据[J].中国地质,46(5):954–976.
- 王铁柱,车林睿,余金杰,陆邦成.2014.宁芜地区梅山铁矿床矿物的电子探针分析和稀土元素地球化学特征[J].中国地质,41(6):1964–1985.
- 吴昌志,张遵忠, Khin Zaw, Fernando Della-pasque, 唐俊华, 郑远川, 汪传胜, 三金柱.2006.东天山觉罗塔格红云滩花岗岩年代学–地球化学及其构造意义[J].岩石学报,22:1121–1134.
- 新疆维吾尔自治区地质调查院.2003.新疆东天山彩霞山—金滩一带靶区优选及资源评价报告[R].1–187.
- 徐璐璐,柴凤梅,李强,曾红,耿新霞,夏芳,邓刚.2014.东天山沙泉子铁铜矿区火山岩地球化学特征、锆石U–Pb年龄及地质意义[J].新疆地质,41(6):1771–1790.
- 徐仕琪,赵同阳,冯京,高永峰,田江涛,杨在峰,刘德权.2011.东天山海相火山岩型铁矿区域成矿规律研究[J].新疆地质,29(2):173–177.
- 曾红,柴凤梅,周刚,耿新霞,李强,孟庆鹏,徐璐璐.2014.新疆雅满苏铁矿床矽卡岩和磁铁矿矿物学特征及其地质意义[J].中国地质,41(6):1914–1928.
- 赵宏军,陈秀法,何学洲,张新元,张潮,王靓靓,陈玉明,陈喜峰,卢民杰,周尚国,黄费新,姚春彦,杨言辰.2018.全球铁矿床主要成因类型特征与重要分布区带研究[J].中国地质,45(5):890–919.
- 张招崇,柴凤梅,谢秋红.2016.热幔–冷壳背景下的高角度俯冲:海相火山岩型铁矿的形成[J].中国地质,(2):367–379.
- 张振亮,冯选洁,高永伟,王志华,董福辰,谭文娟.2015.新疆西天山晚古生代主要磁铁矿床(点)成因类型与成矿过程探讨[J].中国地质,(3):737–758.
- 赵联党,陈华勇,张莉,张增杰,李登峰,张维峰,陆万俭,杨骏,闫学录.2017.新疆黑尖山Fe–Cu (–Au)矿床氢氧同位素特征及其地质意义[J].矿床地质,36(1):38–56.